Using computational fluid dynamics to describe H2S mass transfer across the water–air interface in sewers

Teuber , Katharina; Broecker, Tabea; Bentzen, Thomas Ruby; Stephan, Dietmar; Nützmann, Gunnar; Hinkelmann, Reinhard

Published in:
Water Science and Technology

DOI (link to publication from Publisher):
10.2166/wst.2019.193

Publication date:
2019

Document Version
Accepted author manuscript, peer reviewed version

Using CFD to describe H_2S mass transfer across the water-air interface in sewers

Katharina Teuber (corresponding author)[a]

Tabea Broecker[a]

Thomas Ruby Bentzen[b]

Dietmar Stephan[c]

Gunnar Nützmann[d]

Reinhard Hinkelmann[a]

[a]Chair of Water Resources Management and Modeling of Hydrosystems, Technische Universität Berlin, Berlin, Germany

[b]Department of Civil Engineering, Aalborg University, Aalborg SV, Denmark

[c]Chair of Building Materials and Construction Chemistry, Technische Universität Berlin, Berlin, Germany

[d]Leibniz-Institute of Freshwater Ecology and Inland Fisheries, Berlin, Germany and Humboldt-University of Berlin, Geography Department, Berlin, Germany

E-Mail: katharina.teuber@uwi.tu-berlin.de

Abstract

For the past 70 years, researchers have dealt with the investigation of odour in sewer systems caused by hydrogen sulphide formations and the development of approaches to describe it. The state-of-the-art models are one-dimensional. At the same time, flow and transport phenomena in sewers can be three-dimensional, for example the air flow velocities in circular pipes or flow velocities of water and air in the reach of drop structures. Within the past years, increasing computational capabilities enabled the development of more complex models. This paper uses a three-dimensional two-phase Computational Fluid Dynamics model to describe mass transfer phenomena between the two phases: water and air. The solver has been extended to be capable to account for temperature dependency, the influence of pH value and a conversion to describe simulated air phase concentrations as partial pressure. Its capabilities are being explored in different application examples and its advantages compared to existing models are demonstrated in a highly complex three-dimensional test case. The resulting interH2SFoam solver is a significant step in the direction of describing and analysing H_2S emissions in sewers.

Keywords: H_2S emissions, numerical simulation, Computational Fluid Dynamics (CFD), OpenFOAM

Introduction

Wastewater in sewers undergoes a lot of physical and biochemical processes. One important factor is the formation of hydrogen sulphide (H_2S), which can cause health risks for sewer workers. The tendency of more complex and longer sewer networks can lead to longer retention times, which enhance the emission of H_2S. Climate change at the same time causes higher temperatures in the wastewater, which increases emission rates.

In the past 70 years extensive research has been performed to increase the knowledge on H_2S formations and to develop approaches, which describe the development of odour in sewers (e.g. Gilchrist 1953, Thistlethwayte 1972). The state-of-the-art models, which have been developed within the last 20 years, are horizontal one-dimensional. These are the SeweX model from Australia (Rootsey and Yuan 2010, Rootsey et al. 2012) and the WATS model from Denmark (Hvitved-Jacobsen et al. 2013). Both are not public domain.

An overview of existing model approaches has been given in Carrera et al. (2016) and the need for further research has been highlighted.

To begin with, the mass transfer approach of the existing models is based on the so-called two-film theory, which uses different assumptions. The WATS model additionally uses different approaches to account for turbulent H_2S transfer rates across the water surface in various applications. These different approaches are empirical or theoretical connections between oxygen and H_2S transfer on the one hand and empirical models linking H_2S emissions to flow properties in the pipe on the other hand (Carrera et al. 2016).

Wang et al. (2018) highlight the shortcomings of the two-film theory. It cannot account for local changes of the flow regime or variations of fluid properties. Furthermore, the theory is based on a constant liquid film that can change in real-life conditions due to flow instabilities. The most limiting factor however is assumed to be the one-dimensionality of the approach. More advanced approaches, the penetration theory and the surface renewal theory, can account for the variability of the flux over time but do not account for local variations, the change of fluid properties or flow regimes (Wang et al. 2018). This has already led to wide applications of CFD models for mass transfer applications in the chemical industry (Wang et al. 2018).

Carrera et al (2016) identified the models' lack to describe mass transfer processes across the water surface, the current approaches of which were considered to be simplified, especially when considering hydraulic structures such as gravity sewers, junctions and water falls. Recent research on water falls or drop structures in sewer systems led to improved formulations to account for the effect of local turbulence (Matias et al. 2017), but these approaches are still empirical equations which are fed into the model.

This short overview leads to the question whether a three-dimensional simulation model could help in increasing the process understanding, especially when analysing complex and turbulent flows in a sewer. Another benefit could be the in-depth analysis and design optimization in hotspots of H_2S emissions.

In order to address this question, a volume of fluid (VOF) approach as it is implemented in OpenFOAM's solver interFoam has been chosen to describe the two-phase flow of water and air. This solver has already been used for a number of demanding hydraulic applications (e.g.

Thorenz and Strybny 2012, Bayón et al. 2015) and enables a stable, robust and accurate description of complex flow phenomena.

The VOF method is often used to describe mass transfer processes in CFD applications (Wang et al 2018). Therefore, Haroun et al. (2010a, 2010b) have developed an approach to describe mass transfer processes across the interface between two fluids using the Henry coefficient for the VOF method. This approach has been implemented in OpenFOAM's solver interFoam by Nieves-Remacha et al. (2015), Yang et al. (2017) and Severin (2017), resulting in a solver which will be called interHarounFoam in the following.

A short outline of the driving biochemical processes leading to H_2S formation shall be given to highlight important factors. When anaerobic conditions occur in the wastewater, sulphate-reducing bacteria, which reside in the biofilms of sewer walls can reduce sulphate to sulphide (Sharma et al., 2008). From the biofilm, sulphide is then diffused into the wastewater as H_2S. In the water, equilibrium conditions depending on the pH value and temperature determine which amounts of sulphide are present as H_2S and as bisulphide ion (HS^-), together they are described as total dissolved sulphide. The air-water equilibrium, which can be described by the Henry coefficient for a volatile compound such as H_2S, can cause emissions of H_2S from the water into the air phase. The rate of the transfer process is influenced by factors such as the flow velocities within the different phases, the pH value, temperature and the concentration of oxygen and nitrate. The Henry coefficient describes the relative amount of a volatile compound in the gas phase as a function of its relative occurrence in the water phase under equilibrium conditions and at constant temperature. The temperature dependency of Henry's law can be described by different equations, for example by the van't Hoff equation. The concentration of H_2S in the air phase defines the intensity of odour (Hvitved-Jacobsen et al., 2013).

As this overview of the relevant processes shows, a sole consideration of the Henry coefficient when describing H_2S emissions is not sufficient. Therefore, relevant extensions have been made to the solver, resulting in a new, specialized solver, interH2SFoam. This solver is able to account for the temperature dependency of the Henry coefficient. Further extensions enable the user to describe the equilibrium between HS^- and pH value in the water phase and to compute the partial pressure of H_2S_g in the air phase in ppm in order to gain a better comparability between simulations and measured values. The assessment of turbulent flow effects on mass transfer will be subject to future research.

In the following, after an introduction on the methods used, the capabilities of the interH2SFoam solver are explored in three simple application examples of vertical one-dimensional flow. Then, mass transfer in a rectangular pipe is simulated. In a final example, the new solver is applied to a highly complex sewer geometry.

Methods

Numerical model

OpenFOAM version 2.4.0 has been used for the work presented in this paper. Additionally, a supplementary library called swak4Foam has been used to generate customized function objects to calculate the equilibrium conditions between H_2S and HS^- as well as the partial pressure in the air phase. This approach makes the use of this function optional for the user. Depending on the framework of the model, the user can then decide whether these functions are needed or not. The temperature dependency on the Henry coefficient of H_2S has been directly implemented in the solver and makes a definition of the temperature as an input parameter mandatory.

Hydrodynamic simulations

The mass transfer solvers are based on the two-phase flow solver interFoam which is based on a VOF approach that considers both phases as one fluid with changing fluid properties. One set of Navier-Stokes equations is solved. The volume fraction of a phase is stored as an additional variable and the phases are distinguished by an additional transport equation. The equations are defined as follows (Rusche 2002):

Mass conservation equation:

$$\nabla \cdot \vec{U} = 0 \tag{1}$$

Momentum conservation equation:

$$\frac{\partial \rho \vec{U}}{\partial t} + \nabla \cdot \left(\rho \vec{U} \vec{U}\right) = -\nabla p_{rgh} + \nabla \cdot \left(\mu \nabla \vec{U}\right) + \left(\nabla \vec{U}\right) \nabla \mu - \vec{g} \cdot \vec{x} \nabla \rho \tag{2}$$

Where p_{rgh} is the static pressure minus hydrostatic pressure:

$$p_{rgh} = p - \rho g h \tag{3}$$

Volume of Fluid equation:

$$\frac{\partial \alpha}{\partial t} + \nabla \cdot \left(\alpha \vec{U}\right) + \nabla \cdot \left((1-\alpha)\vec{U}_r \alpha\right) = 0 \tag{4}$$

with the following parameters:

$$\rho = \alpha \rho_{aq} + \rho_g (1-\alpha) \tag{5}$$

$$\mu = \alpha \mu_{aq} + \mu_g (1-\alpha) \tag{6}$$

$$\mu_i = \mu_{i,phys} + \mu_{i,turb} \; with \; i = aq, g \tag{7}$$

where $\vec{U}$ is the velocity field [m/s]; ρ is the density [kg/m^3]; t is time [s]; p is the pressure [Pa]; μ is the dynamic viscosity [Ns/m^2]; $\vec{g}$ is the acceleration vector due to gravity [m/s^2]; $\vec{x}$ is a spatial position vector [m]; α is a volume fraction or indicator function [-]; $\vec{U}_r$ is the relative velocity between the phases [m/s]; the subscripts aq and g denote the fluids water (aq - aqueous) and air (g - gas). For the dynamic viscosity μ, the physical viscosity μ_{phys} and the turbulent viscosity μ_{turb} are considered (see Equation 7).

The indicator function α is defined as:

$$\alpha = \begin{cases} 1 & fluid\ aq \\ 0 < \alpha < 1 & transistional\ region \\ 0 & fluid\ g \end{cases} \quad (8)$$

The water surface is defined as the area where $\alpha = 0.5$.

A turbulence model based on the Reynolds averaged Navier-Stokes equations (Standard k-ε) is applied to consider the turbulent part and the near-wall turbulence is modelled by so-called wall functions. More advanced turbulence models, such as Large Eddy Simulations (LES) or Direct Numerical Simulations (DNS), would offer the opportunity of resolving small-scale velocity variations but would come with the price of a highly increased computation time. As we expect that the application of more advanced turbulence effects would not change the insights on the equilibrium conditions of the mass transfer simulations addressed in this publication, a RANS turbulence model has been considered to be sufficient as well as the best way to save computational resources. Even with the Standard k-ε turbulence model, the computation time of 10 seconds simulation for the complex sewer geometry amounted to 12 hours on 80 parallel processors using the high performance computing (HPC) clusters of TU Berlin.

The accuracy of the hydrodynamic simulations has been assessed in Teuber et al. (in press).

Transport simulations

In general, the transport of a passive tracer with a concentration c is examined with an advection-diffusion equation that can be implemented into the interFoam solver (see Equation 9). The physical diffusivity D_{phys} as well as the turbulent Schmidt number Sc_{turb}, which defines the turbulent diffusivity coefficient D_{turb}, then have to be defined by the user (Equation 10).

Advection-diffusion equation:

$$\frac{\partial c}{\partial t} + \nabla \cdot (\vec{U} c) = \nabla (D_{phys} + D_{turb}) \nabla c \quad (9)$$

with

$$D_{turb} = \frac{\mu_{turb}/\rho}{Sc_{turb}} \quad (10)$$

Mass transfer

Mass transfer has been simulated using the approach defined by Haroun et al. (2010a, 2010b) as it has been implemented by Nieves-Remacha et al. (2015) and Severin (2017). The approach is based on the interFoam solver and considers one additional transport equation for both phases as outlined in Equations 9 and 10.

$$\frac{\partial c}{\partial t} + \nabla \cdot (\vec{U} c) = \nabla \cdot ((D_{phys} + D_{turb}) \nabla c + \phi) \quad (11)$$

A concentration flux expression at the interface results in the following:

$$\phi = -(D_{phys} + D_{turb})(\frac{c(1-He)}{\alpha + He(1-\alpha)})\nabla\alpha \quad (12)$$

167

168 In order to distinguish the species transport between the two phases, Henry's law must be
169 fulfilled and the concentration flux must be consistent:

$$He = \frac{c_{aq}}{c_g} \quad (13)$$

$$(D_{phys,aq} + D_{turb,aq})\nabla c_{aq} = (D_{phys,g} + D_{turb,g})\nabla c_g \quad (14)$$

170 The concentrations and diffusion coefficients are considered as single-phase properties
171 depending on the phase fraction value α:

$$c = \alpha c_{aq} + c_g\,(1-\alpha) \quad (15)$$

$$D_{phys} = (\frac{D_{phys,aq} D_{phys,g}}{\alpha D_{phys,aq} + (1-\alpha) D_{phys,g}}) \quad (16)$$

172 The diffusion coefficients for D_{aq} and D_g are defined by the user. Note that these coefficients
173 are temperature dependent which has to be taken into account when defining the values.

174 **Henry coefficient**

175 The Henry coefficient, also known as Henry constant, is a temperature dependent variable
176 which is reported in many different forms in literature and is often expressed in different units.

177 In this paper, three different definitions of the Henry coefficient are relevant for the derivation
178 and comparison with analytical solutions. Sander (2015) lists values of Henry coefficients in
179 the unit [mol/(m³Pa)] and defines this Henry coefficient as H^{cp}. For the implementation in the
180 interHarounFoam solver, the dimensionless Henry coefficient H^{cc} is relevant (see Equation 13):

$$H^{cc} = He = \frac{c_{aq}}{c_g} \quad (17)$$

181 Where the Henry coefficient is expressed as the ratio between the concentration in the aqueous
182 phase c_{aq} and the concentration in the gas phase c_g.

183 H^{cp} can be converted to H^{cc} using the ideal gas law:

$$H^{cc} = H^{cp} \cdot R \cdot T \quad (18)$$

184 Where R is the universal gas constant $8.314\,\frac{kg\,m^2}{s^2 mol\,K}$ and T is the temperature [K].

185 For H_2S, the Henry coefficient at standard temperature (25 °C) results in:

$$H^{cc}_{H2S} = 10^{-3}\,\frac{mol\ s^2}{m^2 kg} \cdot 8.314\,\frac{kg\,m^2}{s^2 mol\,K} \cdot 298.15\,K = 2.479 \quad (19)$$

186

Extensions

Temperature dependency of Henry coefficient

The Henry coefficient depends on the overall temperature in the domain. Therefore, the temperature dependency has been added in a way that the solver takes one global temperature value as an input parameter.

The temperature dependent Henry coefficient is computed using the van't Hoff equation following Sander (2015):

$$H^{cp}(T) = H^{cp} \exp\left(C\left(\frac{1}{T} - \frac{1}{T^{\theta}}\right)\right) \quad (20)$$

Here, C is a temperature coefficient, which depends on the enthalpy of dissolution and is defined as 2100 K (Sander 2015), T^{θ} is the standard temperature 298.15 K corresponding to 25°C.

Equilibrium conditions

The equilibrium conditions are implemented following Hvitved-Jacobsen et al. (2013). The aim is to describe the water-phase concentration of H_2S depending on the amount of total dissolved sulphide and the pH value since those values are usually measured in field investigations.

The dissociation of H_2S is generally expressed by the following equilibrium:

$$H_2S_g \Leftrightarrow H_2S_{aq} \Leftrightarrow HS^- + H^+ \Leftrightarrow S^{2-} + 2H^+ \quad (21)$$

The equilibrium between H_2S in the gas phase (H_2S_g) and H_2S in the water phase (H_2S_{aq}) is described by the Henry coefficient. In the water phase, an equilibrium between hydrogen sulphide H_2S_{aq} and bisulphide ion (HS^-) exists, where the total amount of both is described as total dissolved sulphide.

Only H_2S_{aq} can be transferred across the air-water interface, not the ionized form HS^-, however, usually the concentration of total dissolved sulphide and the pH value are measured. Therefore it is useful to derive a way to calculate the concentration of c_{H2Saq} when c_S and pH are given.

The equilibrium depends on the equilibrium constant K_{a1} (also known as acid dissociation constant):

$$K_{a1} = \frac{c_{H^+}\, c_{HS-}}{c_{H2Saq}} \quad (22)$$

The dissociation can also be described using the negative logarithm of K_{a1}, pK_{a1} ($pK_{a1} = -\log K_{a1}$), resulting in the Henderson-Hasselbalch equation:

$$log_{10}\, \frac{c_{H2Saq}}{c_{HS-}} = pK_{a1} - pH \quad (23)$$

For a temperature of 20°C the equilibrium constant is $pK_{a1} = 7.0$. Between the ionized form HS^- and the sulphide ion another equilibrium exists in the water phase:

$$HS^- \Leftrightarrow S^{2-} + H^+ \quad (24)$$

$$K_{a2} = \frac{c_{H+} c_{S2-}}{c_{HS-}} \quad (25)$$

The value of pK_{a2} = 14.0 indicates that measurable amounts of the sulphide ion S^{2-} only exist at a value above a pH of about 12. Therefore, only the equilibrium value of K_{a1} is important for wastewater and has been implemented for the interHarounFoam solver in OpenFOAM using the utilities funkySetFields (for initial conditions) and funkySetBoundaryFields (as boundary conditions) from swak4Foam.

The step-by-step reformulation based on Hvitved-Jacobsen et al. (2013) of the equations which results in the equation implemented in OpenFOAM is shown in the following, beginning with the Henderson-Hasselbalch equation:

$$log_{10}\frac{c_{H2Saq}}{c_{HS-}} = pKa1 - pH \tag{26}$$

Solving the log-function and using the expression $c_S = c_{HS^-} + c_{H2Saq}$ for the total dissolved sulphide:

$$10^{pKa1-pH} = \frac{c_{H2Saq}}{c_{HS-}} = \frac{c_{H2Saq}}{c_S - c_{H2Saq}} \tag{27}$$

Rearranging leads to the mass concentration γ_{H2Saq} in [kg/m³]:

$$\gamma_{H2Saq} = \frac{c_S \cdot 10^{pKa1-pH}}{1 + 10^{pKa1-pH}} \tag{28}$$

This can be converted into a molar concentration c_{H2Saq} [mol/m³] by dividing through the atomic weight M_S (0.032 kg/mol) of sulphur (S):

$$c_{H2Saq} = \frac{\gamma_{H2Saq}}{M_S} = \frac{\gamma_{H2Saq}}{0.032\ \frac{kg}{mol}} \tag{29}$$

Thus, the resulting equation implemented in OpenFOAM is:

$$c_{H2Saq} = \frac{\frac{c_S \cdot 10^{pKa-pH}}{1 + 10^{pKa-pH}}}{32} \tag{30}$$

Note that the equilibrium constants K_{a1} and K_{a2} are temperature dependent (Yongsiri et al. 2004), which is not considered in the current version of the code. The value of K_{a1} is a user-defined variable and the temperature dependency of the equilibrium constant has to be accounted for by defining the corresponding K_{a1} value for the temperature analysed.

Calculation of partial pressure of H_2S_g in ppm

The partial pressure of H_2S_g is being computed using a function object in swak4Foam.

The input value in OpenFOAM is a tracer c_{H2Saq} in [mol/m³], requiring a unit conversion:

$$c[\frac{mol}{l}] = 1\frac{mol}{l} = \frac{c_{H2Saq}}{1000} = \frac{1000\frac{mol}{m^3}}{1000} \tag{31}$$

The conversion from ppm to atm is:

$$10^{-6}\ atm = 1\ ppm \tag{32}$$

According to Hvitved-Jacobsen et al. (2013), the partial pressure of a trace quantity in the air phase can be expressed by multiplying the molar concentration with the molar volume:

$$p_{H2Sg}[atm] = c_{H2Saq}[\frac{mol}{l}] \cdot 22.4 \frac{l}{mol} \quad (33)$$

Together, this leads to the following equation for conversion:

$$p_{H2Sg}[ppm] = 10^6 \frac{c_{H2Saq}[\frac{mol}{m^3}]}{1000} \cdot 22.4 \frac{l}{mol} \quad (34)$$

This conversion is only valid for the gas phase concentration, therefore the expression is multiplied with (1-α) in order to keep the conversion constraint to the air phase.

Case studies

In the following, three different cases will be used to explore the possibilities of the existing solver, to validate the new features added to the solver and to show the importance of the model compared to the existing model approaches. For all simulations, at a temperature of 25°C, physical diffusivities for H_2S in water of 2.2 10^{-9} m²/s and in air of 1.74 10^{-5} m²/s are chosen.

The first setup is a quasi-one-dimensional cubic tank with the measures 1m x 1m x 1m bounded by upper, lower and sidewalls with no-slip conditions. The tank is partially filled with water (water depth d = 0.5 m). Both fluids water and air are at rest. As an initial condition, an H_2S concentration of c_{H2Saq} = 1mol/m³ in the water phase is given, the concentration in the air phase is c_{H2Sg} = 0mol/m³. The domain is discretized with 100 cells in y-direction, which is the vertical dimension of the domain, and 10 cells in x- and z-direction. At the bottom wall, a concentration source is assumed, using a fixed value boundary condition of 1 mol/m³. The top wall as well as the sidewalls are defined with zeroGradient conditions. This setup is used to illustrate the solver's capabilities in a simple setup. In a first example, mass transfer, as it can be described with the existing interHarounFoam solver, is shown in a vertical one-dimensional case. Then, the extensions leading to the interH2SFoam solver are demonstrated in different examples using this first setup.

In a second setup, mass transfer in a rectangular duct is analysed using two well-documented examples of water-air pipe flow as they have been described by Bentzen et al. 2016 (test cases no. 7 and 21). The investigated pipe has a length of 15.0m, a height of 0.26m and a width of 0.3m with two different water depths and slopes. The air phase is only accelerated by the movement of the water surface. Bentzen et al (2016) measured resulting velocity profiles in detail using Laser Doppler Anemometry (LDA) velocity measurements. The flow characteristics of the two test cases analysed are listed in Table 1. The setup is a relatively simple three-dimensional setup of a pipe. It illustrates the applicability of the model to regular pipes. The computational domain consists of 307,970 cells. The inlet has been divided in two parts: one for the water phase and one for the air phase. For the water phase, a fixed discharge has been defined, and the phase fraction value α has been defined to be α = 1. The pressure boundary condition has been defined as null Neumann condition. For the air phase, a fixed pressure has been defined and the phase fraction value has been set to α = 0. The velocity has been defined using a null Neumann condition. At the outlet, a free outflow has been assumed. A fixed pressure has been defined and the remaining boundary conditions were defined as null Neumann conditions. At the walls, no-slip conditions were applied. Hydrodynamic simulations (without mass transfer) were run for 200s, until quasi steady state conditions were reached, afterwards a concentration c_{H2Saq} = 1 mol/m³ has been defined for the water at the inlet,

assuming contaminated water flowing into the domain. The upper fluid then has a concentration of c_{H2Sg} = 0 mol/m³ at the inlet, all remaining boundaries were defined with null Neumann conditions.

Table 1. Mass transfer in rectangular channel: flow properties of analysed test cases.

Test no.	Duct slope (%)	Water depth (cm)	U_{aq} (m/s)	U_g (m/s)	Reynolds number Re_{aq}	Reynolds number Re_g
7	0.57	3.15	0.77	0.226	72,300	5,400
21	1.34	4.00	1.37	0.336	175,300	7,900

The third setup describes a complex sewer geometry with an overall length of 93.3m, a width ranging from 6.0m to 7.5m and a sewer height between 4.3m and 5.3m. The setup is shown in Figure 6. This geometry has been simulated in OpenFOAM and compared to experimental results from a 1:20 scale model by Bayón et al (2015) and Teuber et al. (in press). The setup describes a highly three-dimensional pipe diversion, including bends and geometry changes as well as a hydraulic jump. The computational mesh consists of 3,029,223 cells. The setup of boundary conditions is similar to the rectangular pipe of Bentzen et al. (2016). The hydrodynamic model has been simulated for 200s, until steady-state conditions were reached. Then, a concentration c_{H2Saq} = 1 mol/m³ has been defined for the water phase and the simulations using the interH2SFoam solver have been carried out for a simulation time of 10s. A temperature of 25°C is assumed.

The results of the numerical simulations are presented in the following Section.

Results and discussion

Saturation of H_2S in a tank

Mass transfer modelling

In our first test case, we present the application of the model to a vertical one-dimensional problem. It illustrates the advantage of the new model in describing vertical concentration profiles in contrast to the existing horizontal one-dimensional approaches. The simplicity of the test case enables a first illustration of the model's capabilities. The simulation has been carried out assuming normal temperature (25°C).

Figure 1 shows the presence of the two phases within the domain (α = 1: water, α = 0: air) and the development of the concentration profile over time. After t = 50s, a decrease of the overall concentration in the water phase can be observed. This is due to the concentration jump at the interface, which has to be fulfilled by the solver. This concentration jump occurs in the first second due to a direct flux of concentration across the interface. After several seconds, the concentration in the water phase is re-established by the source term at the bottom and after t = 1000s, a steady-state has developed and a constant concentration profile is achieved. The concentration in the water phase is then equal to the source term concentration and the air phase concentration is defined by the Henry coefficient. A detailed validation of the flux under transient conditions has been performed by Haroun et al. (2010a).

The concentration profile illustrates that the resulting air phase concentration is $c_{H2Sg} = 0.4034$ mol/m³, which is the expected concentration in the air phase when applying Henry's law for H_2S:

$$c_{H2Sg} = \frac{c_{H2Saq}}{H_{H2S}^{cc}} = \frac{1\frac{mol}{m^3}}{2.479} = 0.4034\frac{mol}{m^3} \qquad (35)$$

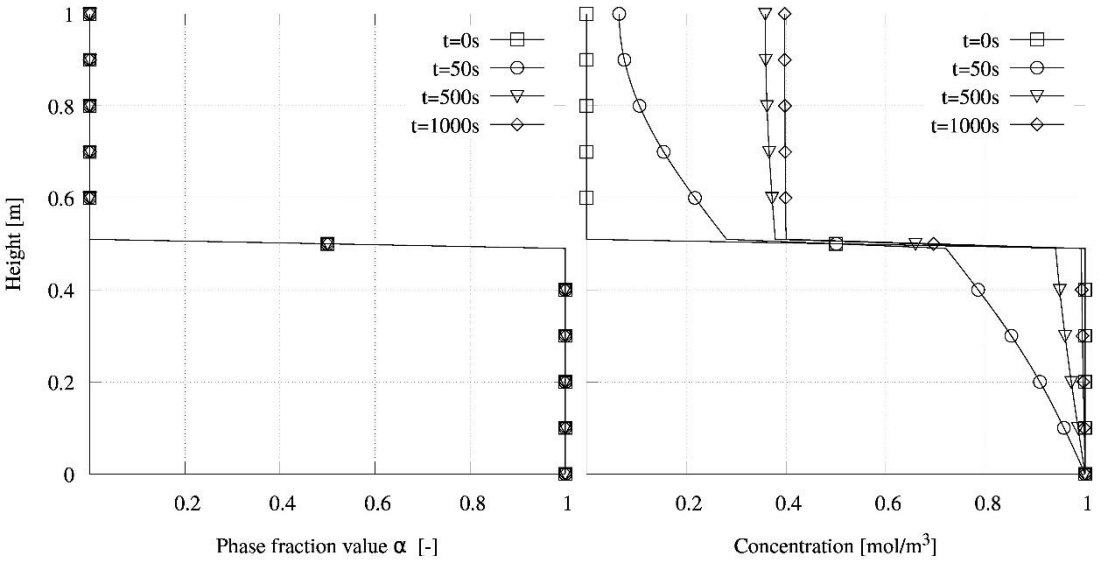

Figure 1. H_2S saturation in a tank (left: phase fraction value, right: concentration profiles along the vertical axis over time).

Temperature dependency

In this test case, we will analytically analyse the temperature dependency of the Henry coefficient, which has been implemented. The application example is based on example 4.2 in Hvitved-Jacobsen et al. (2013). The Henry coefficient at a temperature of 15°C is being calculated.

In this case, a temperature of 288.15 K has been chosen. The resulting Henry coefficient can be determined as follows (following Equations 18-20):

$$H^{cc}(T) = H^{cp} \exp\left(C\left(\frac{1}{T} - \frac{1}{T^{\theta}}\right)\right) R\,T \tag{36}$$

$$H^{cc}(288.15) = 0.001 \cdot \exp\left(2200\left(\frac{1}{288.15} - \frac{1}{298.15}\right)\right) \cdot\ 8.314 \cdot 288.15 \tag{37}$$

$$H^{cc}(288.15) = \ 3.083 \tag{38}$$

Resulting in the following expected gas-phase concentration $c_{H2S,g}$= 0.324 mol/m³:

$$c_{H2Sg}(288.15) = \frac{1}{3.083} = 0.324 \tag{39}$$

Figure 2 shows the resulting concentration in the domain after t = 1000s. The result agrees well with the expected concentration. The implemented temperature dependency can therefore be considered as accurate.

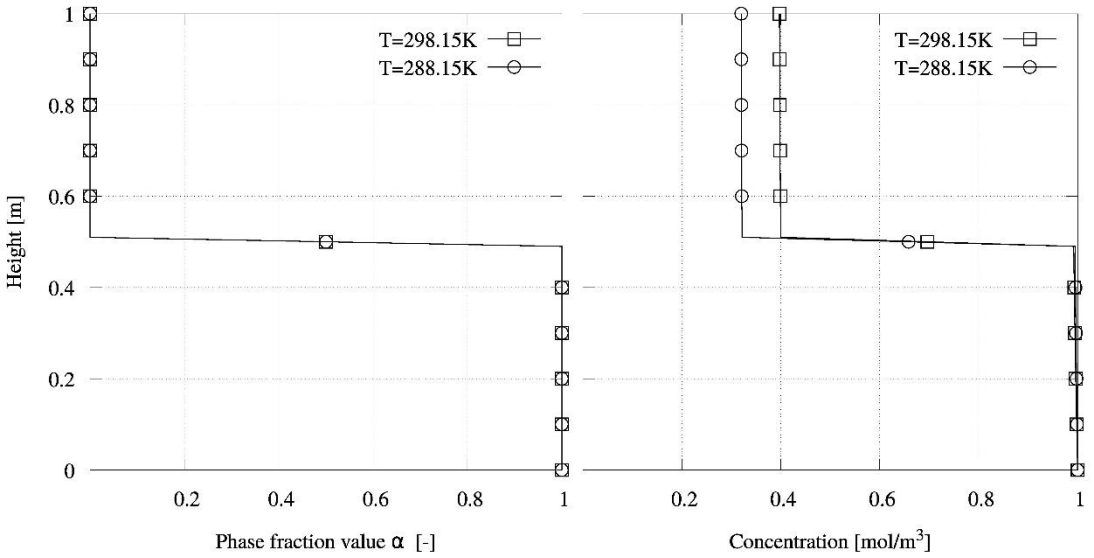

Figure 2. H_2S saturation in a tank for different temperatures (298.15K (cp. Figure 1, right) and 288.15K) (left: phase fraction value, right: concentration profiles along the vertical axis).

Equilibrium conditions and unit conversion

In order to validate the solver extensions regarding the equilibrium conditions and the partial pressure in the air phase, example 4.3 by Hvitved-Jacobsen et al. (2013) is simulated. The resulting H_2S_{aq} and H_2S_g concentrations for a measured concentration of dissolved sulphide c_{S^-} and pH value have been simulated. Again, the basic setup of the case is the same as for the first

application example. A temperature of 15°C, p_{Ka1} = 7.0, pH = 7.0 and a dissolved sulphide concentration of 0.001 kg/m³ are given.

In Hvitved-Jacobsen et al. (2013), the Henry coefficient for the given temperature of 15°C is assumed to be the same as the Henry coefficient from a previous calculation for a temperature of 20°C, i.e. 433 atm. For comparing the analytical solution with the simulated values, the exact Henry coefficient for 15°C has been calculated. Using this value and performing the same calculation steps with the corrected Henry coefficient, the analytical solution leads to a water phase H_2S concentration of c_{H2Saq} = 0.0075 mol/m³, a gas phase concentration of c_{H2Sg} = 0.0027mol/m³ and a corresponding partial pressure of p_{H2Sg} = 66 ppm.

Figure 3 shows the results of the numerical simulations. In the water phase, the concentration of H_2S is c_{H2Sg} = 0.0075mol/m³, in the air phase the concentration reaches a value of c_{H2Saq} = 0.0027mol/m^3 and a corresponding partial pressure (in the gas phase) of p_{H2Sg} = 66 ppm and thus agrees well with the analytical solution. The implemented approach predicts the resulting concentrations accurately.

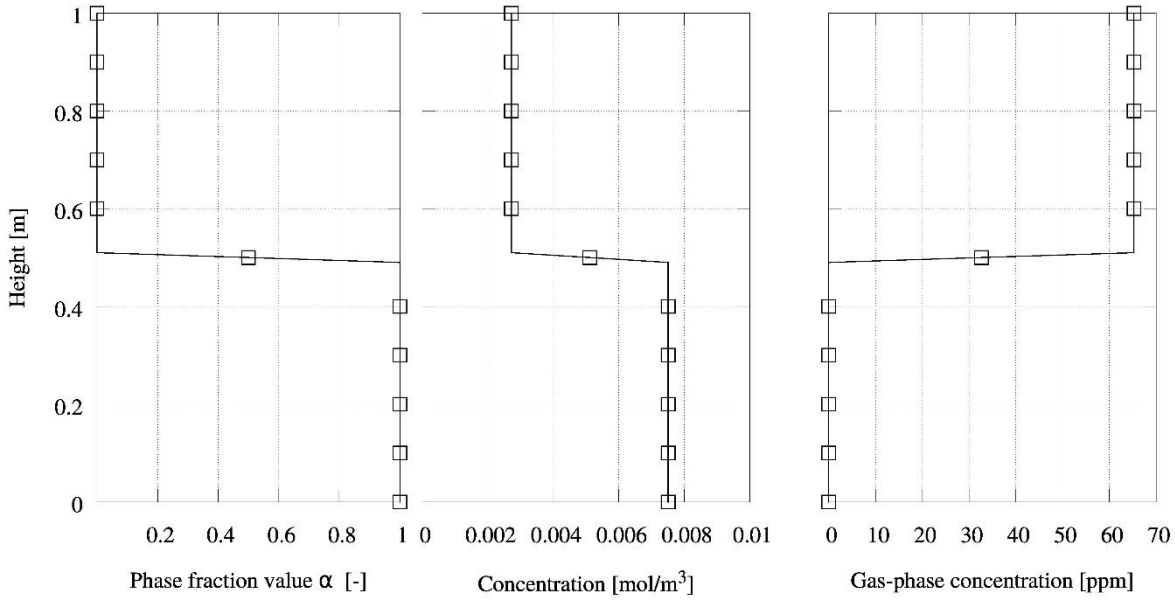

Figure 3. Application example for HS^- and H_2S equilibrium and partial pressure of air phase concentration (left: Phase fraction value profile over domain height, middle: concentration profile in, right: partial pressure of gas-phase concentration).

Mass transfer in a rectangular channel

In this test case, we present mass transfer simulations in a rectangular pipe. Figures 4 and 5 present the resulting phase fraction, velocity and concentration profiles along the height of the domain in the middle of the pipe. The simulated velocity profiles indicate a good agreement with the measured values by Bentzen et al. (2016). For a pipe with a length of 15 m and the analysed flow velocities, the concentration profiles show that almost no mass transfer across the water surface into the air phase can be observed. This can be explained by small velocities in directions other than the main flow direction (i.e. in the yz-plane) which cause advective transport to occur mostly in the main flow direction (x-direction). Furthermore, the small diffusion coefficients cause mainly advective transport. This example opens the question how simulated mass transfer is influenced under highly turbulent conditions or in cases with higher velocities in the yz-plane, which will be analysed in the next example.

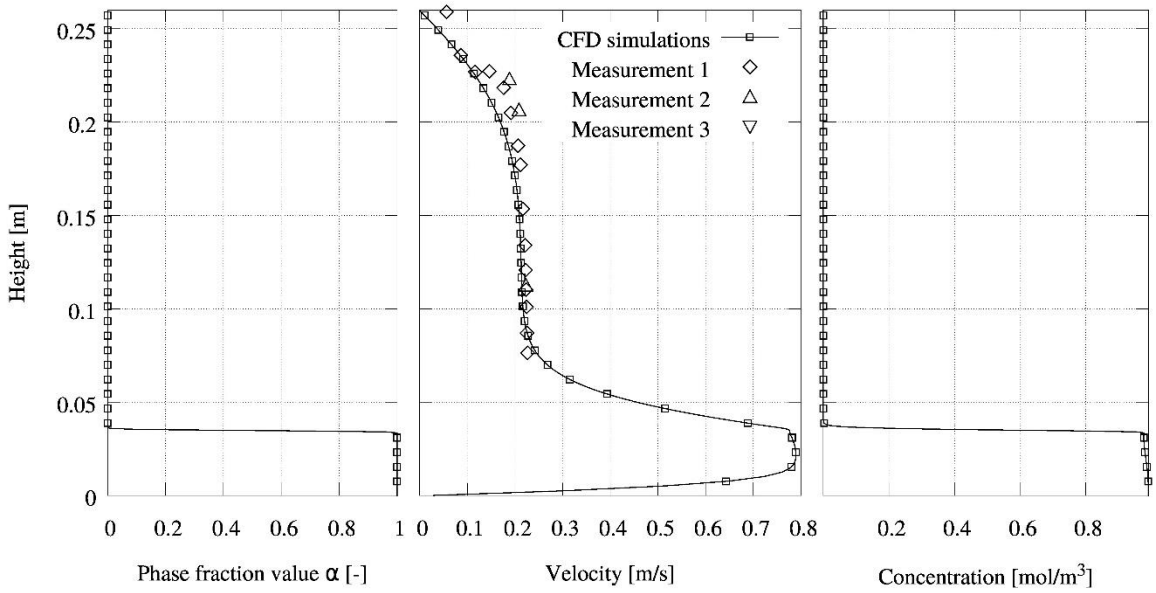

Figure 4. Mass transfer in rectangular channel for test 7 (see Table 1) (left: phase fraction value, middle: velocity, right: concentration profiles).

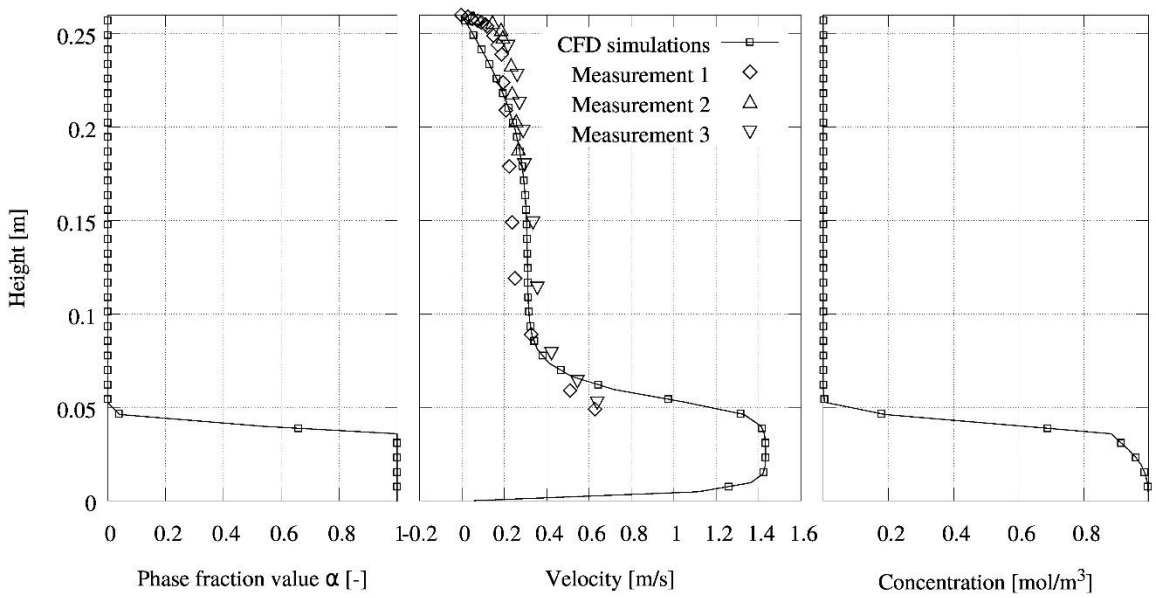

Figure 5. Mass transfer in rectangular channel for test 21(see Table 1) (left: phase fraction value, middle: velocity, right: concentration profiles).

Complex sewer geometry

In a final example, the advantage of the new model are demonstrated by applying the solver to a complex and highly three-dimensional sewer geometry. The existing models are not public domain, therefore a direct comparison to the one-dimensional models is not possible, but the results of the CFD model will be used to highlight the advantages compared to the concepts of the existing approaches.

The results of the simulations at t = 10s are displayed in Figure 6. Figure 6a) gives an overview of the computational domain and the water phase behaviour. The location of highest turbulence occurs in the hydraulic jump, which is displayed in Figures 6b) and 6c). The velocity vectors in Figure 6b) indicate the highly three-dimensional flow behaviour in this location and show the complex water surface movement. In Figures 6c) and 6d), the isosurfaces of the resulting H_2S concentration in the domain are displayed. The concentration range between 0 mol/m³ and 1mol/m³ has been divided into 10 surfaces. The value range in between is not displayed, leaving white spaces for better illustration of the surfaces. The contour plots show, that a more diverse and highly three-dimensional concentration profile develops at the reach of the hydraulic jump. This indicates the increased mass transfer (i.e. higher distance of concentration isolines to the water surface) in the location of the hydraulic jump.

Because the existing model approaches are not public domain, a direct comparison to simulation results is not possible, however, the advantages of the new CFD based mass transfer approach are the following:

(i) In respect to the hydrodynamic behaviour, the new model can describe the three-dimensional flow velocities in the air and water phase. The sewer geometry analysed consists of a bent pipe structure with varying shapes and a hydraulic jump. A hydrodynamic one-dimensional approach would describe this geometry as one connection pipe between beginning and end point. The flow velocity would be

calculated as a uniform value without accounting for the complexity of the geometry. The existing model would not account for the highly complex interaction of water and air phase in the hydraulic jump.

(ii) Regarding the mass transfer, the model would then account for advection and molecular diffusion and for turbulence in the free-stream flow areas as well as in drop structures in a very simplified way. This would lead to a simplified assumption of the actual mass transfer occurring in the pipe, since the effect of turbulence on the mass transfer is substantial. A validation of the actual mass transfer rate due to turbulence effects is performed in Teuber et al. (under review).

Most sewer stretches in urban areas are not as complex as the previously shown example and wide networks without high levels of turbulence justify the use of one-dimensional models. However, locations of high turbulence can enhance H_2S emissions and the three-dimensional approach presented in this paper can help analyse the effect of local design aspects on the resulting H_2S emissions and improve the sewer network design.

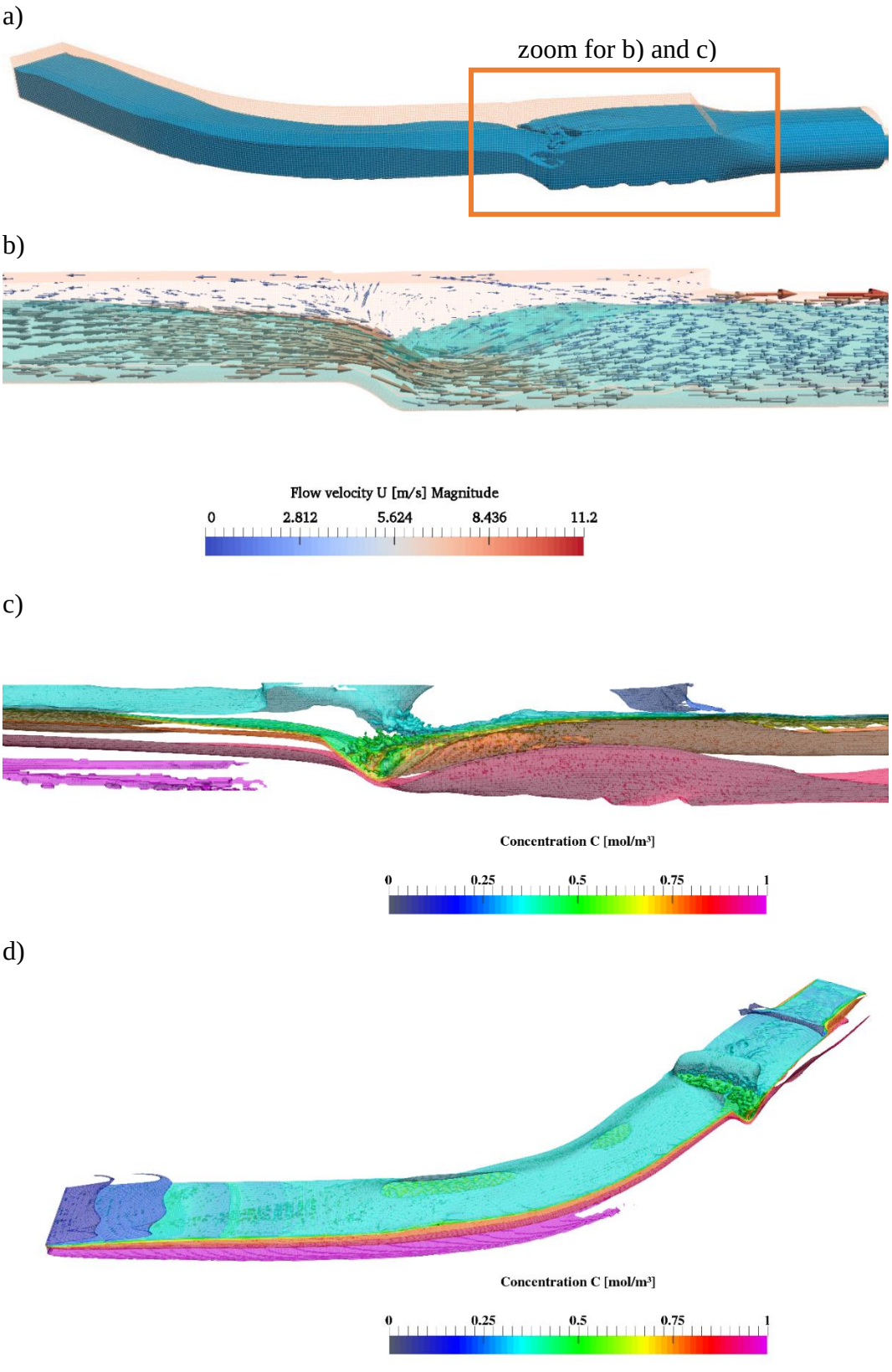

Figure 6. Mass transfer simulations in complex sewer geometry at t=10s (a) overview of the domain filled with water under steady-state conditions, b) flow velocities and water surface behaviour in hydraulic jump, c) top view on tracer distribution, d) tracer distribution in hydraulic jump).

Conclusions

H_2S emissions and their consequences are an important topic when considering urban drainage and the design of sewer networks. In the past, different model approaches, from empirical to conceptual, have been developed in order to describe and predict H_2S emissions and resulting odour. These models are horizontal one-dimensional, therefore neglecting the occurrence of three-dimensional effects.

In this publication, a model approach has been introduced that can describe H_2S emissions across the water surface using a mass transfer approach based on the Henry coefficient, which is implemented in the open source software OpenFOAM. Two-phase flow has been simulated using a VOF method. The solver has been extended by different key features that are crucial when describing H_2S emissions. The temperature dependency of the Henry coefficient has been taken into account. Equilibrium conditions between HS^- and H_2S are described and enable the usage of the measured value for total dissolved sulphide and the pH value as input parameters. The solver also computes the partial pressure of H_2S in the gas phase based on the simulated concentration of H_2S_g.

The new solver has been applied to different simple test cases and the results have been compared to analytical solutions. Furthermore, it has been applied to a highly complex three-dimensional test case to highlight the advantages of the new model approach. Compared to one-dimensional formulations, it can account for highly complex flow effects in a sewer stretch and describe mass transfer in such environments. The analysis of the results showed an increased mass transfer in the location of highest turbulence, which agrees with existing observations. The exact quantification of local mass transfer rates has been validated in Teuber et al. (under review) and has led to a good agreement with experimental results.

Overall, the new solver enables an analysis of mass transfer in complex three-dimensional test cases, the description of which has so far only been possible with major simplifications.

Future research will deal with further extensions of the solver to account for temperature effects in the fluids and reactive transport modelling.

Acknowledgements

The complex sewer geometry has been computed on the supercomputers of Norddeutscher Verbund für Hoch- und Höchstleistungsrechnen in Berlin.

The funding provided by the German Research Foundation (DFG) within the Research Training Group ‘Urban Water Interfaces’ (GRK 2032-1) is gratefully acknowledged.

We thank Prof. Arnau Bayón for providing the experimental data and the mesh for the complex sewer geometry.

References

Bayón, A., Vallés-Morán, F. J. & López-Jiménez, P. A. 2015 Numerical analysis and validation of South Valencia sewage collection system diversion. In: *36th IAHR World Congress*, The Hague, Netherlands.

Bentzen, T. R., Østertoft, K. K., Vollertsen, J., Fuglsang, E. D. & Nielsen, A. H. 2016 Airflow in Gravity Sewers - Determination of Wastewater Drag Coefficient. *Water Environment Research*, **88**(3), 239-256.

Carrera, L., Springer, F., Lipeme-Kouyi, G. & Buffiere, P. 2017 Sulfide emissions in sewer networks: focus on liquid to gas mass transfer coefficient. *Water Science and Technology*, **75**(8), 1899-1908.

Edwini-Bonsu, S. & Steffler, P. M. 2006 Dynamics of air flow in sewer conduit headspace. *Journal of Hydraulic Engineering*, **132**(8), 791-799.

Gilchrist, F.M.C. 1953. Microbiological studies of the corrosion of concrete sewers by sulphuric acid producing bacteria. *South African Journal of Chemistry*, 214–215.

Haroun, Y., Legendre, D. & Raynal, L. 2010 Volume of fluid method for interfacial reactive mass transfer: application to stable liquid film. *Chemical Engineering Science*, **65**(10), 2896-2909.

Haroun, Y., Legendre, D. & Raynal, L. 2010 Direct numerical simulation of reactive absorption in gas–liquid flow on structured packing using interface capturing method. *Chemical Engineering Science*, **65**(1), 351-356.

Hvitved-Jacobsen, T., Vollertsen, J. & Nielsen, A.H. 2013 Sewer processes: microbial and chemical process engineering of sewer networks, 2nd edn., *CRC press*.

Matias, N., Nielsen, A. H., Vollertsen, J., Ferreira, F. & Matos, J. S. 2017 Erratum: Water Science and Technology 75 (10), 2257–2267: Liquid-gas mass transfer at drop structures. *Water Science and Technology*, **76**(6), 1584-1594.

Matias, N., Nielsen, A.H., Vollertsen, J., Ferreira, F. & Matos, J. S. 2017 Liquid-gas mass transfer at drop structures. *Water Science and Technology*, **75**(10), 2257–2267.

Nieves-Remacha, M.J., Yang, L. & Jensen, K.F. 2015 OpenFOAM computational fluid dynamic simulations of two-phase flow and mass transfer in an Advanced-Flow Reactor. *Industrial & Engineering Chemistry Research*, **54**(26), 6649-6659.

Rootsey, R. & Yuan, Z. 2010 New insights into sewer odour and corrosion. In: *6th International Conference on Sewer Processes and Networks*, Queensland, Australia.

Rootsey, R., Melchers, R., Stuetz, R., Keller, J. & Yuan, Z. 2012 Taking control of odours and corrosion in sewers. In: *Australia's National Water Conference and Exhibition (OzWater 2012)*, Sydney, Australia.

Rusche, H. 2003 *Computational fluid dynamics of dispersed two-phase flows at high phase fractions*, PhD thesis, Imperial College London (University of London), London, United Kingdom.

Sander, R. 2015 Compilation of Henry's law constants (version 4.0) for water as solvent. *Atmospheric Chemistry and Physics*, **15**, 4399-4981.

Severin, T. S. 2017 *Computational Fluid Dynamics Assisted Design of Thin-Layer Cascade Photobioreactor Components*, PhD thesis, Technische Universität München, Munich, Germany.

Teuber, K., Broecker, T., Bayón, A., Nützmann, G. & Hinkelmann, R. (in press) CFD-modelling of free-surface flows in closed conduits. *Progress in Computational Fluid Dynamics*.

Teuber, K., Broecker, T., Nützmann, G. & Hinkelmann, R. (under review) CFD simulation of H2S mass transfer under turbulent conditions in a stirring tank, *submitted to Water Science and Technology on April 12, 2019*.

Thistlethwayte, D. K. B. 1972 Control of sulphides in sewerage systems. *Ann Arbor Science*.

Thorenz, C. & Strybny, J. 2012 On the numerical modelling of filling-emptying systems for locks. In: *Proceedings of the 10th International Conference on Hydroinformatics (HIC)*, Hamburg, Germany.

Wang, C., Xu, Z., Lai, C. & Sun, X. 2018 Beyond the standard two-film theory: Computational fluid dynamics simulations for carbon dioxide capture in a wetted wall column. *Chemical Engineering Science*, **184**, 103–110.

Yang, L., Nieves-Remacha, M. J. & Jensen, K. F. 2017 Simulations and analysis of multiphase transport and reaction in segmented flow microreactors. *Chemical Engineering Science*, **169**, 106-116.

Yongsiri, C., Vollertsen, J. & Hvitved-Jacobsen, T. 2004 Effect of temperature on air-water transfer of hydrogen sulfide. *Journal of Environmental Engineering*, **130**(1), 104-109.